Single channel atmospheric pressure transporting plasma and plasma stream demultiplexing: physical characterization and application to E. coli bacteria inactivation

Azade Valinataj Omran, F Sohbatzadeh, S N Siadati, A Hosseinzadeh Colagar, Y Akishev, Farzaneh Arefi-Khonsari

Single channel atmospheric pressure transporting plasma and plasma stream demultiplexing: physical characterization and application to *E. coli* bacteria inactivation

A Valinataj Omran [1, 2, 3], F Sohbatzadeh [3, 5], S N Siadati [3], A Hosseinzadeh Colagar [4, 5], Y Akishev [6, 7] and F Arefi-Khonsari [1, 2]

[1] Sorbonne Universités, UPMC Univ Paris 06, UMR 8235, Laboratoire Interfaces et Systèmes Electrochimiques, 75005 Paris, France

[2] CNRS, UMR8235, LISE, F-75005 Paris, France

[3] Department of Atomic and Molecular Physics, Faculty of Basic Sciences, University of Mazandaran, Babolsar 47416-95447, Mazandaran, Iran

[4] Department of Molecular and Cell Biology, Faculty of Basic Sciences, University of Mazandaran, Babolsar 47416-95447, Mazandaran, Iran

[5] Nano and Biotechnology Research Group, Faculty of Basic Sciences, University of Mazandaran, Babolsar 47416-95447, Mazandaran, Iran

[6] SRC RF TRINITI, 108840, Russia, Moscow, Troitsk, Pushkovykh Str., vladenie 12

[7] National Research Nuclear University MEPhI, 115409, Russia, Moscow, Kashirskoe sh.-32

E. mail: f.sohbat@umz.ac.ir, a_valinataj@hotmail.com

Abstract

In this article, we developed transporting plasma sources that operate at atmospheric pressure. The effect of electrode configuration on plasma transporting was investigated. In order to increase the transporting plasma cross section, we converted a plasma stream into four plasma channels by a cylindrical housing. Electron-excitation and rotational temperatures were estimated using optical emission spectroscopy. Furthermore, the electrical and temporal characteristics of the plasma, discharge power and charge deposition on the target were investigated. The propagation characteristics of single and multi-channel transporting plasma were compared with the same cross-section area. Two configurations for multi-channels were designed for this purpose. *Escherichia coli* bacteria were exposed to the single and multi-channel transporting discharge for different time durations. After exposure, the results indicated that the inactivation zones were significantly increased by a multi-channel transporting plasma. Finally, *E. coli* inactivation by those plasma apparatuses was compared with that of several standard antimicrobial test discs such as Gentamicin, Tetracycline, Amoxicillin and Cefixime.

1. Introduction

Atmospheric-pressure room-temperature plasma jets have attracted a lot of attention for numerous applications in plasma medicine [1–5], surface and materials processing [6–9]. Although the discharges in

plasma jets typically appear as continuous plasma, high-speed imaging shows that the plasma in fact comprises discrete, fast moving plasma bullets [10–12], or ionization waves (IWs). The plasma jet strongly resembles the cathode-directed streamers in some aspects, and some authors speculated that it may be initiated in a way independent of the capillary dielectric barrier discharge [13]. The propagation of the IWs is responsible for transporting the associated intense electric field, and creating charged and neutral excited species and UV photons at remote locations.

The propagation of plasma bullets in a cold plasma jet has been widely studied, and the influence of the discharge parameters on the plume characteristics has been reported [14–19]. In order to meet adequately various customers' needs, it is necessary to develop different plasma sources, especially, those which can generate long transporting plasma strings meant for treatment of remote downstream targets. The transporting plasma (TP) is a cold plasma source allowing the propagation of plasmas inside long dielectric capillaries. Aiming to be specifically and locally delivered, such technology drives the plasma up to the target where the plasma is transferred in ambient air at the outlet of the capillary. However, there are few reports dealing with the TP or in other words, propagation of IW through a dielectric tube [20–23], and the mechanisms about the formation of ionization waves inside a dielectric tube still remain unclear. Especially, the effect of electrode structure on the propagation of IW through long dielectric tube needs to be further investigated. Our previous study [24] showed that the high voltage excitation waveform is crucial for the ignition of He long plasma strings. The effect of the tube diameter on the transported plasma was also examined: the lower the diameter, the higher the applied voltage. Noble gas plasma jets applied to large area surface processing remain a big challenge, because the cross sections of the atmospheric pressure plasma jet plumes are typically small. One promising way to overcome this shortcoming is using the plasma jet arrays. However, since the individual plasma plumes generated by the arrayed plasma jets are in most cases independent and do not merge in open air, it is very difficult to achieve uniform plasmas and surface treatment effects.

Robert et al. developed a first version of low temperature plasma, "plasma gun," traveling through capillary tube [21]. The plasma gun device is then used as a single primary discharge reactor likely to drive the operation of multi jet arrays [25].

In this paper, in the first part, the influence of electrode configuration on the transporting discharge has been studied. Since in many atmospheric plasma applications the gas temperature has a crucial role, its accurate measurement is very important to optimize the process performance. Rotational temperature and also excitation temperature of TP were estimated by Boltzmann plot. The second part of this paper is dedicated to the development and characterization of transporting multi-channel structures as a generalization of a single transporting plasma source. The characteristics of a single and multi-channel TP were compared with the same cross-section area. To better understand the formation and propagation in tubes and in ambient air, the discharge characteristics of the TP arrays were investigated by electrical and

optical apparatus. The third part of this paper describes the potential of TP devices in developing bacteria decontamination systems.

2. Effect of electrode structure in single TP

2.1. Experimental setup

Figure 1 presents the schematic of the experimental set up. To investigate the role of different electrode configurations on single TP, two different electrode structures were used: single electrode and double electrodes DBD like jets.

The single electrode structure for the single TP is made of a 2 mm inner diameter and 4 mm outer diameter of Pyrex tube with a steel pin wire as the powered electrode. The helium flow is fed through the reactor tube with a flow rate in the order of 2 slm. The working gas was controlled through a mass flow controller (Beijing Seven star Electronics Co., Ltd, D07-19B) and flow readout box (Beijing Seven star Electronics Co., Ltd, D08-1F). The plasma device was driven by a homemade power supply with an AC high voltage at 5 kHz which was superimposed on a DC high voltage. The double electrode structure for the single TP is shown in figure 1(b).

In both setups the steel pin wire was set to be the powered electrode and the ground electrode wrapped around the dielectric tube in a double electrode configuration.

The sample was placed on the grounded aluminum plate one cm away from the exiting TP to study *E.coli* inactivation (Figure 1(b)).

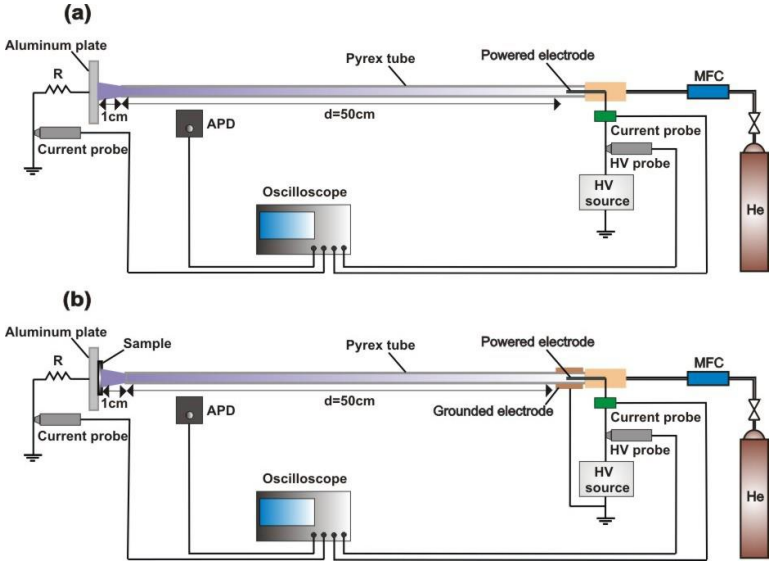

Figure 1. Scheme of two structures for single TP (a) single electrode and (b) double electrode.

In figure 1, experimental setup for voltage, current signals and avalanche photodiode detector (APD) measurements were depicted. The plasma ionization wave radiation was captured by the APD (Thorlabs, 110A2/M, 200-1000 nm) with bandwidth of DC-50MHz and rise time of 7 ns in different positions along its path and also between the nozzle and the ground plane. The current and applied voltage were measured

with a wideband current probe (Pearson Electronics, Inc., model 3972) and a high voltage probe (Tektronix P6015A, Tektronix, Inc.), respectively. The collected signals were recorded by a digital oscilloscope. Also, the charge transferred to the aluminum grounded plate was measured with a shunt resistor.

The plasma emission was measured using an optical fiber located downstream at 15 mm from the nozzle exit and connected to two different Ocean Optics spectrometers (HR2000+ and Maya 2000 Pro). The first one had a grating of 1800 g/mm (res_{th}=0.035 nm) in the blue range (300–430 nm) and the second one 300g/mm (res_{th}=0.1 nm) in the visible spectrum range, both with a slit of 25 micrometers.

2.2. Electrical Characteristics

The results showed that the plasma ignition voltage in the double electrode setup is lower than the single electrode one, suggesting a much higher electric field at a given applied voltage. This is because the single electrode structure had a floating ground of uncertain physical location and its inter-electrode distance was likely to be larger than that of the double electrode.

Figure 2 shows the typical waveforms of the applied voltage and current signals for both setups which were measured by Pearson current monitor. Additionally, in order to study the time behavior of the TP which consists of ionization waves, we monitored the radiation of the TP outside the nozzle, between the nozzle outlet and ground plane, by the APD. It was observed that the discharge produced one ionization wave in each cycle of the applied AC voltage which was recorded by its radiation.

Thus, the velocity of ionization wave in air for single electrode and double electrodes was measured by using the delay between the APD and shunt resistor signals. Thanks to the stable operation of the TP, the propagation velocity of the plasma stream in air was estimated to be about 78 km/s for double electrodes and 83 km/s for single electrode. As can be seen in figures 2(b) to 2(d), the ionization wave initiates earlier in the double electrode configuration in a single TP.

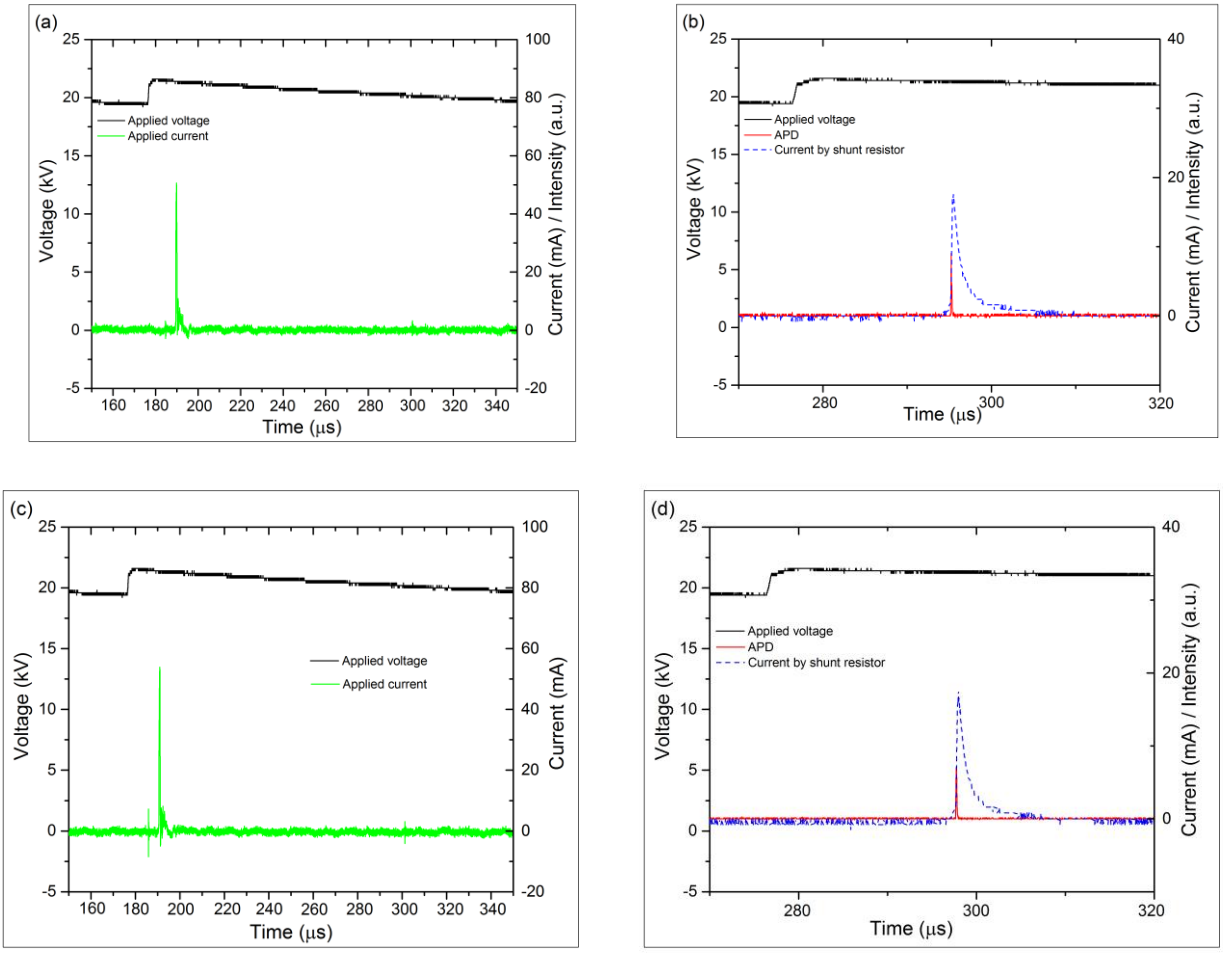

Figure 2. Voltage waveform, current signal, current on shunt resistor and corresponding photodiode signal (a) & (b) double electrodes and (c) & (d) single electrode configuration.

For processing applications, the most relevant issue is the amount of reactive plasma species delivered to the sample. An estimation was made for the total charge transfer (q) to the grounded plate using a shunt resistor by using the following equation:

$$q=\int I\,dt \qquad (1)$$

In which I is the current signal recorded by the shunt resistor based on ionization wave impinging to the grounded plate. The applied power on the high voltage electrode, using a Pearson current monitor, the deposited charge on the grounded plate, the dissipated power measured by means of the shunt resistor and the ionization wave velocity in air at the exit (the space between the tube exit and grounded plate (placed one cm away)) were estimated and the results were shown in Table 1.

Table 1. Estimated applied power, charge deposition, dissipated power by the shunt resistor and velocity of ionization wave in two electrode structures in a single TP.

	Double electrodes	Single electrode

Applied power on the HV electrode (W)	3.7	3.28
Deposited Charge (nC)	31±1	26±2
Dissipated Power by the shunt resistor (mW)	1.06±0.01	1±0.03
Velocity of ionization wave in air (km/s)	78±6	83±1

It is seen that the transferred charge to the grounded plate in double and single electrode structures are 31.15 and 26.52 nC, respectively. This suggests that the double electrode structure is more efficient in producing electrons and in turn more reactive species.

2.3. Propagation velocity inside the tube

The ionization wave velocity was measured along the TP by means of APD signals. By placing the APD at different positions along the tube, the signals were captured and restored, and then the velocities were calculated from the delay time at different locations. It reaches a peak velocity of about 96 km/s near the nozzle outlet. Figure 3 shows the APD signals for different locations along the TP.

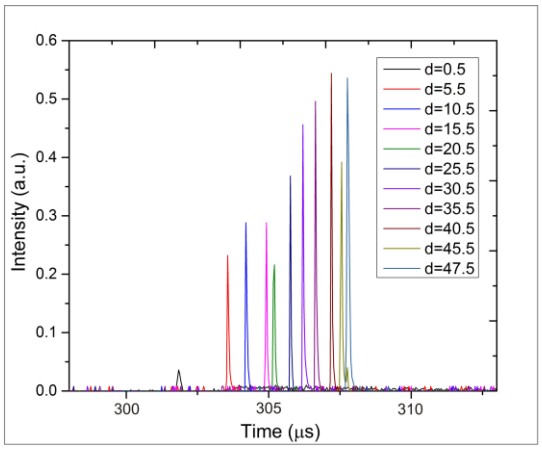

Figure 3. Optical emission of plasma ionization wave recorded by APD along the tube in single electrode configuration as a function of the distance d from the powered electrode.

Figure 4 indicates that the ionization wave accelerate toward the tube exit after initiation from the powered electrode. This feature is different from those reported by Robert, 2009 and Mussard, 2013 where the velocities of the ionization waves either decrease or stay constant at first before increasing [21,26].

Robert and his group [21] presented the evolution of the speed of the transient plasma burst in neon plasma gun. They used two similar photodiodes set a few centimeters apart along the dielectric guide. A strong decrease of the propagation speed was observed with 10 times reduction from 10 to 55cm positions. The highest velocity value was measured at 10 cm distance from the electrode tip to be of 2500 km/s for neon flushed glass capillary, by changing the position to 55cm the velocity decreased dramatically. Mussard et al [26] used the multi-antenna system to measure velocities which was between 5-200 km/s

and it was shown that the discharge accelerates when it crosses the discontinuity during the propagation of a ionization wave.

The linear increase of the propagation length during the cycle is interpreted as the deposition of positive charges that create a region of high potential on the whole propagation distance.

The potential gradient between the two regions—a region of high potential at the vicinity of the powered electrode and a low potential region around the grounded plate—implies the existence of a DC induced electric field parallel to the tube axis which is much larger in amplitude than the Laplacian field correlated with the voltage applied on electrode. This electric field which arises from our excitation waveform (ac voltage superimposed on DC) is responsible for such acceleration mechanisms.

But it was shown by Bourdon et al [27] that the ionization wave propagation velocity is correlated with the applied voltage. The time evolution of axial and radial components of the electric field measured by an electro-optic probe set outside the tube are compared with simulation results. Both, simulations and measurements in the tube or within the plasma plume show peak electric fields of the order of 45 kV/cm.

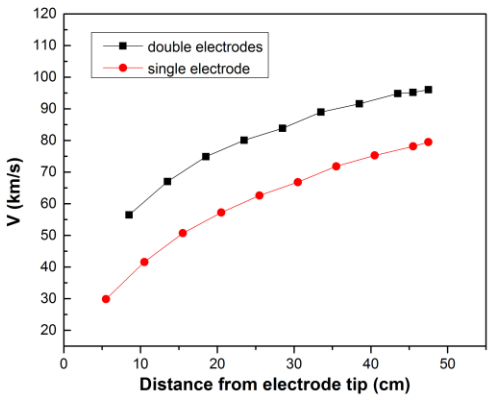

Figure 4. The velocity of ionization waves propagating along the tube as a function of the location along the axis of the tube for the single and double electrode configurations.

This result confirms that TP is propagating at a much higher velocity than the gas in the confined environment of the capillary.

The propagation velocity of the ionization wave is strongly determined by the electron drift velocity $v_e = \mu_e E$, where μ_e is the electron mobility and E is the local electric field. The electron mobility μ_e in turn depends on the gas composition. When the gas leaves the tube, it intermixes more and more with the surrounding air. Therefore the electron mobility decreases and leads to a reduction in the propagation speed of the ionization wave in the space between the tube exit and grounded plate.

2.4. Temperature measurement

Since the discharge operates in open air, impurities are always present in the atmospheric pressure plasma jet. The gas temperature is usually obtained by means of the rotational temperature of some molecular species present in the discharge such as OH species [28–30] and N_2^+ [31,32] on account of the highly favorable energy exchange of heavy particles and the internal rotational–vibrational states of the molecular species involved [33]. Assuming that these molecules are in equilibrium with the gas atoms, the rotational temperature derived from the rovibrational spectra can be considered as equal to the gas temperature. This assumption is reliable for atmospheric pressure plasmas since the exchange between the translational energy of the molecules and their internal rovibrational states is very efficient [34]. In our experiments, molecular N_2^+ and OH bands were observed in the spectra. However, the intensity of the OH band was too weak to enable sensitive measurements of the rotational distribution, hence of the gas temperature.

The emission bands of the second positive system of nitrogen N_2 ($C^3\Pi_u - B^3\Pi_g$) at rovibrational transitions at (0–2), (1–3) and (2–4) from 368 to 382 nm are used and simulated by the software Specair [35] to determine the rotational (T_{rot}) and vibrational (T_{vib}) temperatures of nitrogen.

The emission spectrum ranging from 300-400 nm and fitting the experimental spectra with the simulated ones are shown in Figure 5. The fitting gives the following vibration and rotation temperatures: T_{vib} = 3500 K, T_{rot} = 300 K. Owing to fast collisional relaxation at atmospheric pressure, the gas temperature T_{gas} equals with T_{rot}. Vibrational temperature $T_{vib} > T_{rot}$ indicates the non-equilibrium in the plasma.

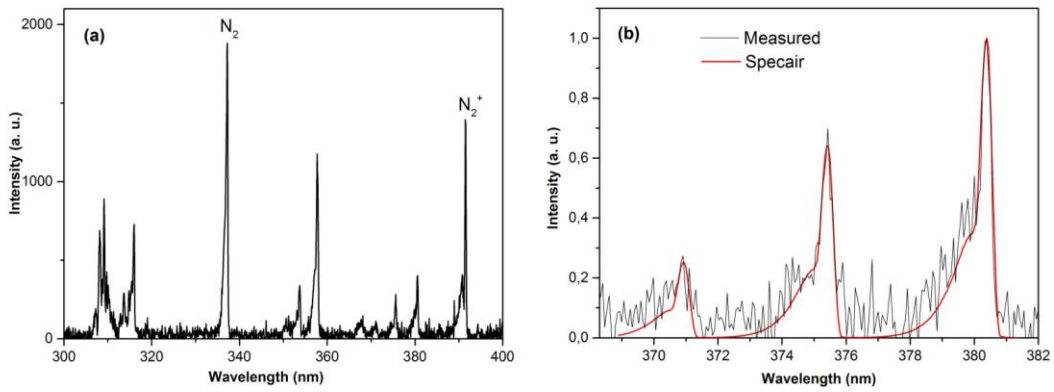

Figure 5. (a) Optical emission spectra obtained from a TP in the range from 300-400 nm and (b) using Specair simulation of the nitrogen emission in the spectral region from 368 to 382 nm.

For determination of the field strength, the ratio $R_{391/337}$ can be known as a function of the electric field strength [36]. In our spectrum, the dependence of the intensity ratio of the nitrogen bands on the field strength in air is determined by of E/N value.

According to the nitrogen bands, the intensity ratio $R_{391/337}$ = 0.742. Comparing to Paris et al works, we have got an extremely high magnitude of the reduced electric field E/N: E/N = 1500 Td. In our opinion, a reason is that this approach does not work in the case of discharge in He. In this discharge the processes of

ionization and excitation of the $C^3\Pi$ states in N_2 are strongly influenced by helium metastables but not direct electron impacts [27].

One of important plasma parameters is the free electron temperature T_e, which is of importance for the evaluation of excitation and ionization rates of plasma species but it is difficult to be measured directly [37].

In low temperature plasmas, the excitation temperature (T_{exc}) derived from the Boltzmann plot [38] should be equivalent to the electron temperature (T_e) [39–41]. T_{exc} for the transporting discharge has been determined from the emission intensities of helium lines.

The He excitation temperature, T_{exc}, was determined from a Boltzmann plot by plotting the quantity $I_{ij}\lambda_{ij}/A_{ij}g_i$ corresponding to various He transitions from upper state i to lower state j, as a function of energy E_i of the respective upper state [42]. Other quantities were I (the recorded intensity), λ (the wavelength), A (the Einstein coefficient) and g (the statistical weight). The following He emission lines were used in the calculation of excitation temperature: 501.6, 587.6, 667.8, 706.5 and 728.2 nm. The Einstein coefficients and statistical weights of these lines were obtained from the National Institute of Standards and Technology (NIST) atomic spectra database [43]. Figure 6 shows the optical emission spectrum in the ranges from 200 to 1000 nm and Boltzmann plot; the corresponding temperature was about 7190±5 K.

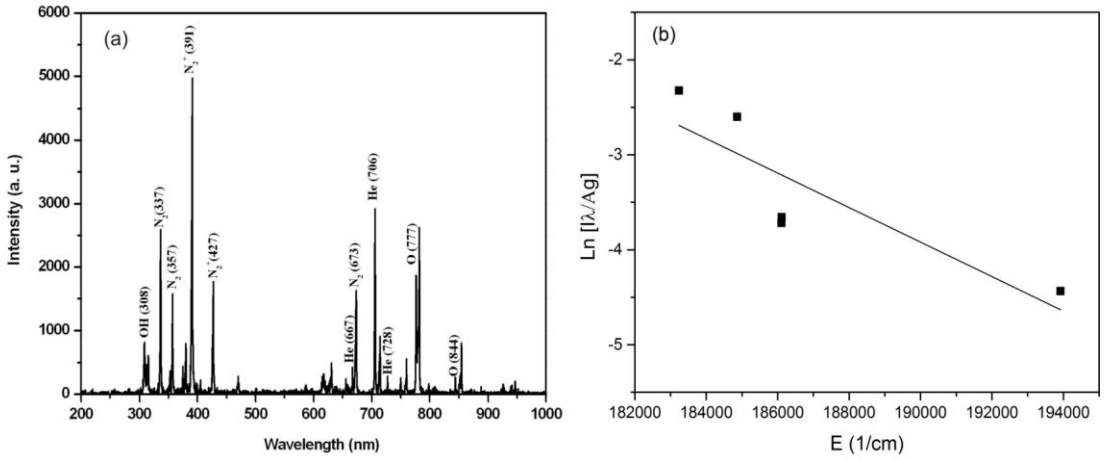

Figure 6. (a) Spectra recorded from the transporting plasma (b) Boltzmann plot for determining He excitation temperature.

3. Multi-Channel Transporting Plasma

In this section, we developed transporting plasma arrays and compared with a single channel TP. Two structures were designed for this purpose, the cross section of each channel in the multi-channel TP was the same as the single TP. Figures 7(a) and 8(a) demonstrate the layout of the two structures for the TP array: bundled transporting plasma (BTP) and demultiplexer transporting plasma (DTP).

In the first structure (figure 7), four channels were bundled in a honeycomb-pattern and four steel pin wires were installed as powered electrodes. All the pin wires were connected to the same high voltage output. A copper tape, 20 mm wide, was wrapped around the bundle as a ground electrode. Each channel was a Pyrex glass tube with 4 mm outer diameter and 2 mm inner diameter. The bundle was connected to the gas flow control by a flexible plastic tube.

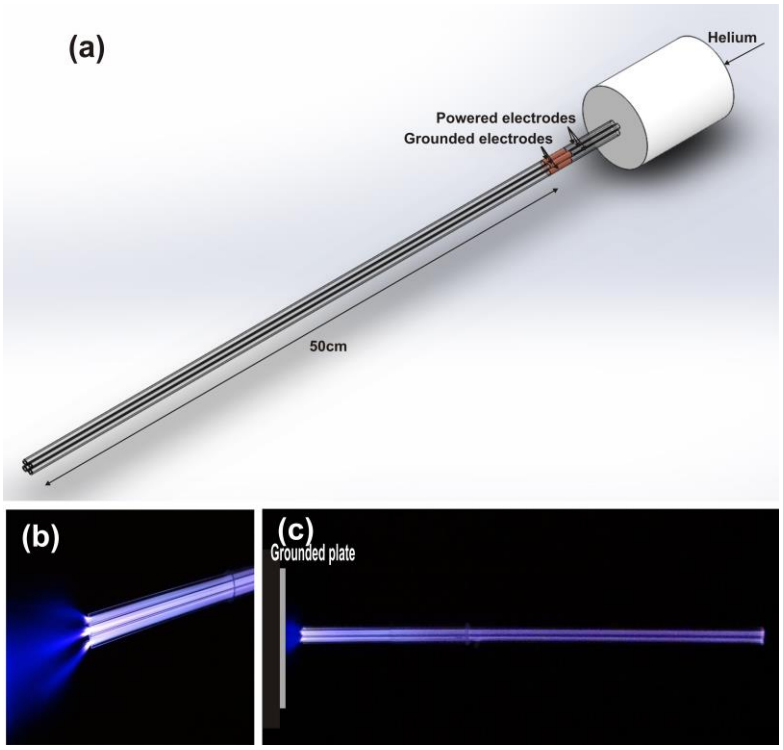

Figure 7. (a) layout of the first structure for BTP, (b) & c) Photographs of first BTP having four powered electrodes

The second structure (Figure 8) comprised of an upstream channel and four downstream Pyrex channels with 4 mm outer diameter and 2 mm inner diameter. The upstream channel was coupled to the 4 downstream ones by a plastic housing serving as the channel demultiplexer. There is no electrode inside the plastic housing nor the downstream channels while the power and the ground electrodes were installed in the upstream channel.

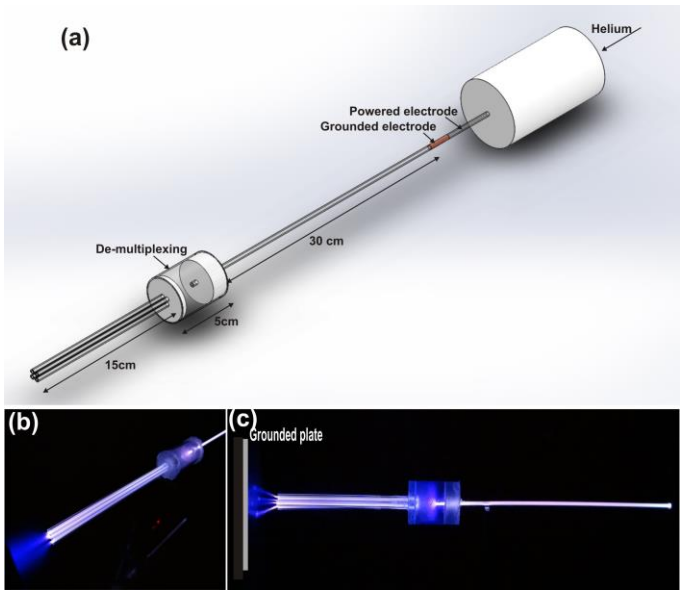

Figure 8. (a) layout of the 1-to- 4 demultiplexer TP, (b) & (c) Photographs of the second structure of DTP.

In order to recognize more the 1-to-4 demultiplexer TP, we developed another single TP (STP) having a Pyrex channel with 50 cm length, 4 mm inner diameter and 6 mm outer diameter. The installed electrodes for the STP were the same as that of the BTP, i,.e. there were a tin steel wire and a copper tape used as the powered and grounded electrodes, respectively.

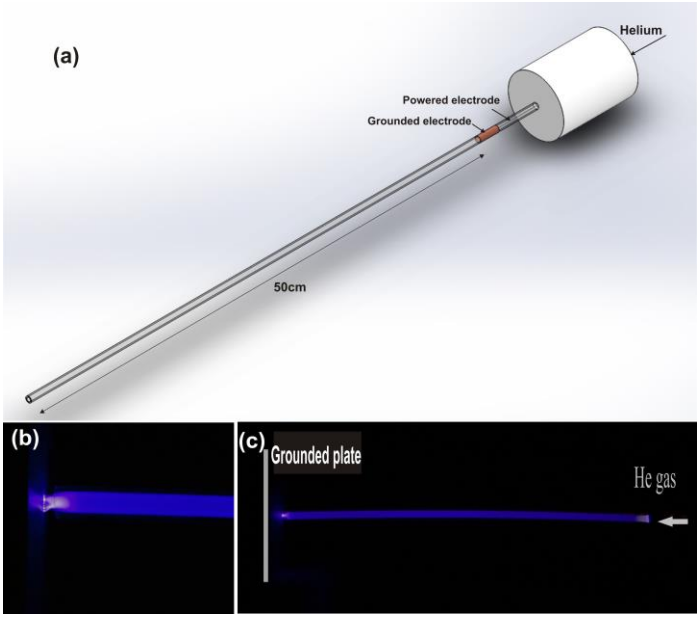

Figure 9. (a) Sketch of the single TP, (b) & (c) Photographs of single TP.

The driving conditions for the multi-channel TPs and the STP were 5 kHz oscillating high voltage which was superimposed on 15 kV positive direct current and 3.8 SLM Helium gas. Once the TPs was created and stabilized, they were placed one cm away from the grounded aluminum plate.

The interaction among the emerging plasma plumes from multi-channel TPs was clearly observed in which they repelled each other due to electrostatic repulsive forces. The latter results from the existence of

a net charge density at the head of the atmospheric-pressure IWs. The net charge density is in part the source of the large *E*/*N* at the head of the IW that sustains the electron avalanche [44].

3.1. Characterization of multi-channel TPs

In this section, we describe the characteristics of DTP and BDP devices. The measured voltage and current waveforms of the multi-channel TPs were shown in figure 10. Note that the charge and power deposition on the grounded plate for STP is smaller than that of multi-channel TPs.

Again, we placed the APD outside the nozzle and used the delay between the signal of APD and shunt resistor for measuring the plasma jet velocity in air. The results showed that the current and APD signals from the BTP were stable and had a good uniformity, as shown in figure 10(c), (d). In addition, there was a delay time between the four ionization wave and in fact four distinct peaks appeared.

In figure 10(f) current signals measured by shunt resistor were shown for DTP. Three distinct current spikes were clearly seen which is another strong evidence of multiple ionization waves propagating in the downstream channels, thanks to demultiplesing behaviour in this category. It is noteworthy that only three current peaks were measured because the fourth bullet did not reach the grounded plate as depicted in figure 10(f).

In the arrays, before the multi-plumes reached to the grounded aluminum plate, the four plasma plumes merged together and formed a uniform plasma layer with a surface cross section of 4 cm^2, as shown in figures 7 and 8.

Compared to the STP, the DTP was brighter and covered a bigger surface. This representation shows that 1-to-4 demultiplexer TP of this size enabled to produce an intense plasma with a significant improvement over STP.

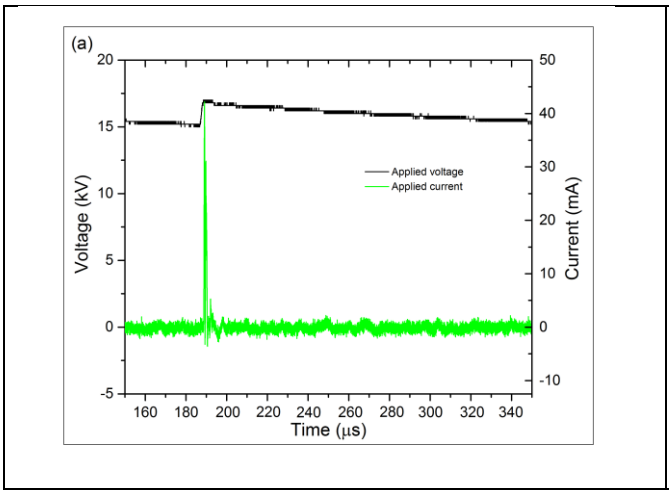

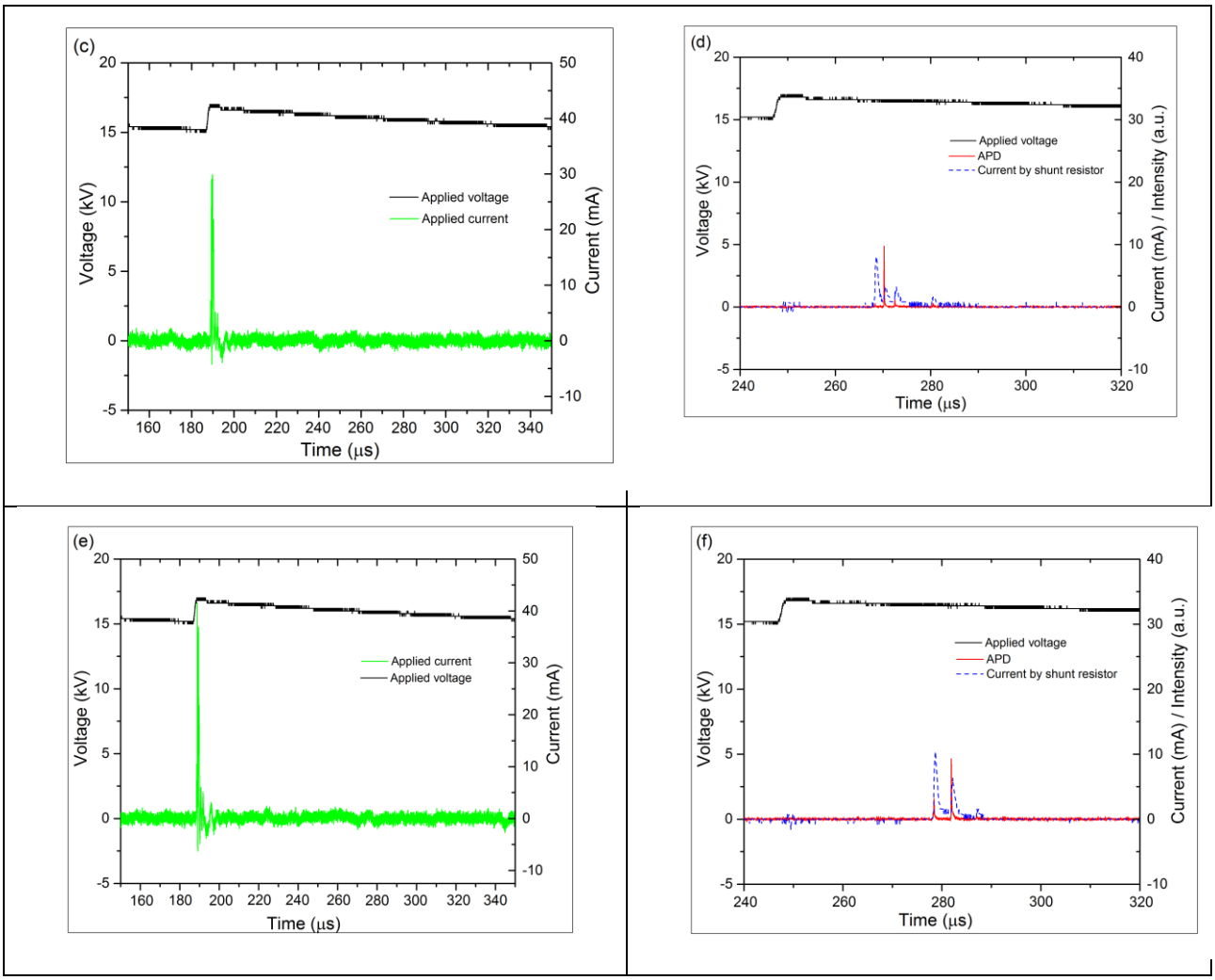

Figure10. Voltage waveform, total current, current on shunt resistor and corresponding photodiode signal (a) & (b) STP (c) & (d) BTP (e) & (f) DTP.

To better understand the TP arrays, the applied power on the high voltage electrode, the charge deposited on the grounded plate, the power measured on the shunt resistor and the velocity of the ionization waves in air have been compared for different conditions (Table 2). Comparing the results for the three investigated conditions, the 1 to 4 demultiplexer TP showed the higher charge, power and velocity values, as compared to the STP.

The transporting plasma takes the form of the ionization waves which constitute the fundamental structure of the streamers. Once IWs launched, they define their own properties through the self-sustaining E/N produced by the space charge in the ionization wave. The charge accumulation on the surface of the tubes has a crucial role on transporting and sustaining the discharge.

Table 2. Calculated applied power, charge and power deposited on the grounded plane and velocity of the plasma in the arrays and the single jet.

	Single TP	BTP	DTP
Applied power on the high voltage electrode (W)	2.85	1.86	1.95
Charge deposited (nC)	11±2	Q_{tot}=13±2	Q_{tot}=14±1.1
		q_1=6±1, q_2=2±1.2	q_1=8±1, q_2=5±0.5
		q_3=2±0.8, q_4=1±0.1	q_3=0.5±0.1
Power deposited (mW)	0.169±0.002	P_{tot}=0.21±0.01	P_{tot}=0.33±0.004
		P_1=0.17±0.01,	P_1=0.25±0.003,
		P_2=0.022±0.003	P_2=0.077±0.002
		P_3=0.016±0.0006,	P_3=0.0002±0.00
		P_4=0.003±0.0004	
Velocity of ionization wave in air (km/s)	31±3	V_1=70±7, V_2=66±5	V_1=86±10, V_2=82±2,
		V_3=75±11, V_4=118±16	V_3=195±17

4. Bacteria Decontamination

Since several years a number of activities on the field of antibacterial treatment by using non-thermal plasmas are known. Atmospheric pressure plasma jet is one of the most efficient sources for decontamination [45–48].

To estimate biological effects of the TP, bactericidal activity was tested as an easy to realize screening method. *E. coli* is a test microorganisms often used for basic plasma source characterization [49,50]. In many cases, oxygen radicals are reported to be one of the important contributors to sterilization [51,52].

For studying the oxygen effect, only a small fraction of oxygen was added to the supplying helium gas in order to generate chemically active species. As predicted by prior literature on plasma-based sterilization, the introduction of a small amount of oxygen in the helium flow actually increased the efficacy of the plasma inactivation [45,47].

The developed STP and multi-channel TPs were used to inactivate *E. coli* bacteria on a solid surface. The working gas (99%He+1%Oxygen) was introduced into the annular space. By supplying the high voltage driver, cold atmospheric pressure TPs were stably produced, moved through the long channels and directed toward the contaminated petri dishes that were located at a distance of one cm from the nozzle.

The material of the target significantly affects the plasma propagation, reactive species and electric field [53–55]. In our experiments, the strong differences appear in the plasma properties when the plasma gets in contact with a solid medium instead of Aluminum ground.

4.1. Bacteria Sample Preparation

A lyophilized bacterial strain of *E. coli* ATCC 35218 was obtained from the Pasteur Institute of Iran. At first, 1 ml of fresh Luria–Bertani (LB) broth was added into lyophilized bacterial strain vial and grown at

37 °C for 16 h with gentle shaking. Afterwards, 500 µl of cultured LB broth was inoculated onto LB agar containing the following components per liter of distilled water: 10 g Bacto Tryptone, 5 g yeast extract, 10 g NaCl, and 15 g agar. After the incubation, one loop from bacteria inoculated to 15 ml LB broth and incubated overnight at 37 °C with gentle shaking. In order to make bacterial suspension, 1 ml of overnight cultured LB broth was transferred to 15 ml of fresh LB broth and incubated at 37 °C until OD_{600nm} reaches to 0.25. The culture, containing approximately 2×10^9 cfu ml^{-1}, was diluted with fresh LB broth to 2×10^8 cfu ml^{-1}.

In order to decontaminate solid surface (LB agar), 100 µl of the diluted suspension containing bacterial concentration of 2×10^8 cfu ml^{-1} was evenly spread over each LB agar plate in Petri dish and left to dry in a laminar flow cabinet at 25 °C for 20 min. Moreover, one control Petri dish was prepared. Petri dishes were exposed to the helium transporting plasma for various durations and then incubated at 37 °C for 16 h. To quantify the decontamination efficiency, the area of inactivation zone was measured.

To determine the approximate area of growth inactivation zones (in square millimeter), the radius of the inactivation zone (r_i), radius of Petri dish (r_p), and area of inactivation zone (πr_i^2) were calculated for each sample. The radius and the area of Petri dishes were 35 mm and 3,846.5 mm^2, respectively. The percentage of inactivation zone was calculated by the following formula: Inactivation zones%$=\pi r_i^2/\pi r_p^2\times100$.

4.2. Inactivation by single transporting plasma

The bacteria were exposed to the single transporting plasma for 0, 3, 6 and 9 minutes. After the exposure of the solid samples to the transporting discharge, round transparent areas marked the growth inactivation zones and were compared with the antibiogram disc diffusion method. For this purpose 2×10^9 colonies of *E. coli* were spread on the general Luria Bertani (LB) solid medium. Then the plasma treated samples compared to the inhibition effects of several antibiotics discs including: Gentamicin (GM), Cefixime (CFM), Tetracycline (TE), Amoxicillin (AMX) and Ampicillin (AM).

To evaluate the effect of different bactericidal antibiotics, the antibiotics discs of gentamicin, Cefixime, Tetracycline, Amoxicillin, Ampicillin with concentrations of 10, 5, 30, 25 and 10 micrograms per disc, respectively, were placed on the surface of the plates containing the bacteria spread. After 16 hours of incubation at 37 °C, growth inhibitions zone of discs were measured using AutoCAD software.

The plasma exposure areas were expanded with increasing time exposure (figure 11) and inactivation zones showed in figure 12. As expected, a clear bactericidal effect of plasma treatment was observed. The magnitude of this effect depends on the treatment time. The results showed that Cefixime antibiotic has the highest effect on the growth of bacteria.

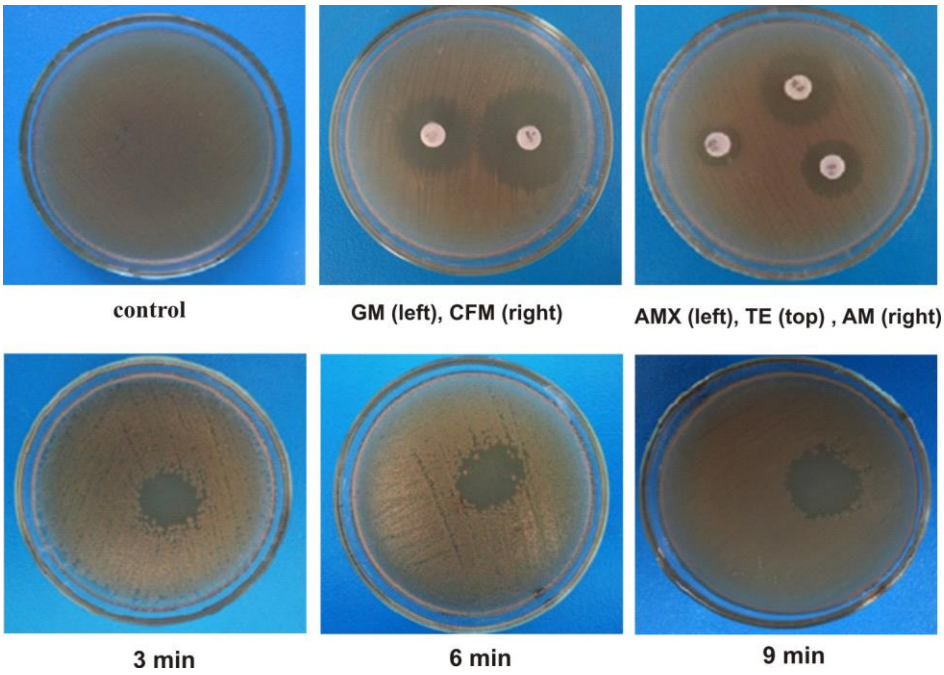

Figure11. The zones of bacterial growth inactivation following exposure to transporting discharge and antibiotics. Concentration of antibiotic per disc including: Am=10µg Ampicillin; GM=10µg Gentamicin; TE=30 µg Tetracycline; AMX=25 µg Amoxicillin; CFM=5 µg Cefixime.

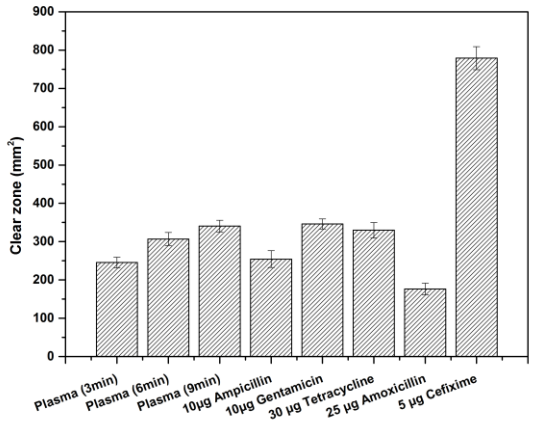

Figure 12. The growth inhibitions zone of bacteria after plasma exposure and antibiogram.

Note that the size of inhibition zone by transporting plasma was always larger than TP cross section. As shown by Lu, 2008 and Goree, 2006, oxygen-reactive species generated by the plasma jet such as O, and O_3, can diffuse radially outward and consequently deactivate cells [2,56]. On the other hand, UV photons produced in atmospheric plasma jets propagate preferentially along the plasma column thus they interact only with a part of the target surface located just under the jet [57]. Therefore, judging by the size of the inhibition zone (much larger than the plasma column diameter) one can conclude that the reactive oxygen and nitrogen species (RONS) produced by jet– surrounding air interactions are the major inactivation agents. As shown in [58] by model simulation of the gas flow dynamics of He/O_2 plasma jet and oxygen

reaction kinetics the O atoms formed in the discharge can propagate over a limited area with a maximum diameter of about several millimeters. However, ozone, which is well known for its bactericidal effect and is stable enough to survive the transport, can inactivate cells at larger distances from the plasma jet [59]. Therefore, it can be concluded that the bacteria in our experiments were deactivated by the reactive oxygen and nitrogen species (RONS).

4.3. Inactivation by demultiplexer and bundle TPs

Furthermore, the decontamination effectiveness of the multi-channel TPs at the channels end was evaluated by direct exposure towards a contaminated agar plate. The treatment took place for 3, 6 and 9 min at a distance of 10 mm from the nozzle exit. The plates were incubated at 37 °C overnight to allow growth. Figure 13 shows that the DTP has better disinfection ability against *E. coli* bacteria compared to the BTP. Also, the decontamination effect by STP in 3 minutes looks better than by DTP and BTP that it can probably explained by repulsions of the jets and the latter had an effect on bactericidal ability of these plasmas.

All samples exhibited egg-like inhibition zones. In the center a combination of all microbicidal agents (VUV, UV, radicals, charged particles) appeared, resulting in the highest reduction factor. In the periphery region only radicals with long life time were present. Hence, the reduction factor is much lower. These results indirectly prove the assumption that the combination of all active agents is most prominent.

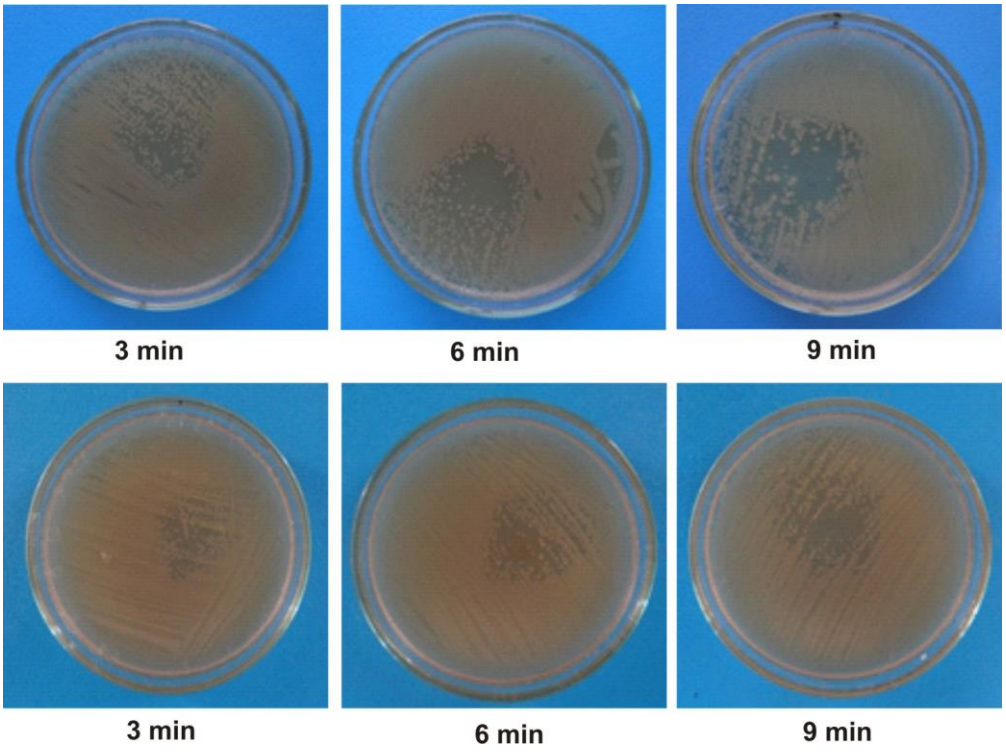

Figure 13. The growth inhibitions zone of bacteria after exposure to DTP (up) and BTP (down) for different exposure times.

5. Conclusion

Atmospheric pressure transporting plasma is a novel way for delivering active species to remote sites for applications such as biomedical procedures, particularly in endoscopic applications and has been the topic of much interest recently.

In this work, long atmospheric pressure cold plasmas was developed using different electrode configurations through single and multi-channel dielectric tubes. The transporting plasmas comprised of discrete ionization waves that originate from the powered electrode, travel the entire tube and diffuse into the ambient air as a cold plasma jet. The gas temperature and electron excitation temperature were estimated from the Boltzmann plot and were around 294 and 7190 K, respectively, which demonstrate the low-temperature feature of the TP.

Scaling the large area atmospheric pressure plasma jet arrays remains a key challenge due to electrical and hydrodynamical coupling between individual plasma jets. Here, we presented a novel means with which one can obtain a large-volume and large-surface-area atmospheric transporting plasma plume array. Two different structures for multi-channel transporting plasmas were designed and their characteristics such as velocity, charge and power deposition on the grounded plate were compared with a single transporting plasma with the same cross-section. A freshly designed multi-channel device was robust and exhibited plasma stability maintaining efficient reaction chemistry and a low gas temperature. Multiple plasma plumes were generated and propagated to the grounded surface uniformly without an auxiliary circuit. The power consumption of these multi-channel plumes were very low, nevertheless they produced intense plasma with a significant improvement over a single TP.

The transporting discharge was cold enough to be put in direct contact with heat sensitive materials. Therefore, by using this approach a transporting plasma was generated inside a tube far from the high-voltage discharge region, which provided the safe operation conditions and device flexibility required for medical treatment.

Furthermore in this work the possibility to direct the excited species of the transporting discharge to the *E. coli* bacteria was shown. We confirmed that *E. coli* bacteria decontamination after 3, 6 and 9 min was comparable with the effect of various antibiotics. Also the bactericidal effect of the multi-channel transporting plasmas was examined.

In addition, the characteristics of the long distance plasma delivery, high density of reactive species, and low temperature allow such plasma sources to be quite suitable for biomedical endoscopic applications.

References

[1] Laroussi M 2009 *IEEE Trans. Plasma Sci.* **37** 714–25
[2] Lu X, Ye T, Cao Y, Sun Z, Xiong Q, Tang Z, Xiong Z, Hu J, Jiang Z and Pan Y 2008 *J. Appl. Phys.* **104** 053309
[3] Kim J Y, Ballato J, Foy P, Hawkins T, Wei Y, Li J and Kim S O 2011 *Biosens. Bioelectron.* **28** 333–8
[4] Keidar M, Walk R, Shashurin a, Srinivasan P, Sandler a, Dasgupta S, Ravi R, Guerrero-Preston R and Trink B 2011. *Br. J. Cancer* **105** 1295–301
[5] Kong M G, Kroesen G, Morfill G, Nosenko T, Shimizu T, Van Dijk J and Zimmermann J L 2009 *New J. Phys.* **11** 115012
[6] Babayan S E, Jeong J Y, Tu V J, Park J, Selwyn G S and Hicks R F 1998 *Plasma Sources Sci. Technol.* **7** 286–8
[7] Tu V J, Babayan S E, Jeong J Y and Sch A 2001 *Plasma Sources Sci. Technol.* **10** 573–8
[8] Pulpytel J, Kumar V, Peng P, Micheli V, Laidani N and Arefi-Khonsari F 2011 *Plasma Process. Polym.* **8** 664–75
[9] Dowling D P, O'Neill F T, Langlais S J and Law V J 2011 *Plasma Process. Polym.* **8** 718–27
[10] Teschke M, Kedzierski J, Finantu-Dinu E G, Korzec D and Engemann J 2005 *IEEE Trans. Plasma Sci.* **33** 310–1
[11] Mericam-Bourdet N, Laroussi M, Begum a and Karakas E 2009 *J. Phys. D. Appl. Phys.* **42** 55207
[12] Walsh J L, Iza F, Janson N B, Law V J and Kong M G 2010 *J. Phys. D. Appl. Phys.* **43** 75201
[13] Sands B L, Ganguly B N and Tachibana K 2008 *Appl. Phys. Lett.* **92** 2006–9
[14] Jarrige J, Laroussi M and Karakas E 2010 *Plasma Sources Sci. Technol.* **19** 65005
[15] Yousfi M, Eichwald O, Merbahi N and Jomaa N 2012 *Plasma Sources Sci. Technol.* **21** 45003
[16] Naidis G V. 2011 *Appl. Phys. Lett.* **98** 76–9
[17] Lu X, Laroussi M and Puech V 2012 *Plasma Sources Sci. Technol.* **21** 34005
[18] Robert E, Sarron V, Darny T, Riès D, Dozias S, Fontane J, Joly L and Pouvesle J-M 2014 *Plasma Sources Sci. Technol.* **23** 12003
[19] Siadati S N, Sohbatzadeh F and Alavi S K 2015 *Phys. Scr.* **90** 85602
[20] Xiong Z and Kushner M J 2012 *Plasma Sources Sci. Technol.* **21** 34001
[21] Robert E, Barbosa E, Dozias S, Vandamme M, Cachoncinlle C, Viladrosa R and Pouvesle J M 2009 *Plasma Process. Polym.* **6** 795–802
[22] Clément F, Svarnas P, Marlin L, Gkelios A and Held B 2011 *IEEE Trans. Plasma Sci.* **39** 2364–5
[23] Kostov K G, Machida M, Prysiazhnyi V and Honda R Y 2015 *Plasma Sources Sci. Technol.* **24** 25038
[24] Sohbatzadeh F and Omran A V 2014 *Phys. Plasmas* **21** 1–8
[25] Robert E, Darny T, Dozias S, Iseni S and Pouvesle J M 2015 *Phys. Plasmas* **22**122007
[26] Dang Van Sung Mussard M, Guaitella O and Rousseau A 2013 *J. Phys. D. Appl. Phys.* **46** 302001
[27] Bourdon A, Darny T, Pechereau F, Pouvesle J-M, Viegas P, Iséni S and Robert E 2016 *Plasma Sources Sci. Technol.* **25** 35002
[28] García M C, Yubero C, Calzada M D and Martínez-Jiménez M P 2005 *Appl. Spectrosc.* **59** 519–28
[29] Christova M, Castanos-Martinez E, Calzada M D, Kabouzi Y, Luque J M and Moisan M 2004 *Appl. Spectrosc.* **58** 1032–7
[30] Muñoz J, Dimitrijević M S, Yubero C and Calzada M D 2009 *Spectrochim. Acta - Part B At. Spectrosc.* **64** 167–72
[31] Muñoz J, Margot J and Calzada M D 2010 *J. Appl. Phys.* **107** 083304
[32] Rodero A, Quintero M C, Sola A and Gamero A 1996 *Spectrochim. Acta - Part B At. Spectrosc.* **51** 467–79
[33] Boumans P W J M 1987 *Inductively coupled plasma emission spectroscopy. Part II: applications and fundamentals*
[34] Moussounda, P. S., Ranson, P., & Mermet J M 1985 *Spectrochim. Acta Part B At. Spectrosc.* **40** 641–51
[35] Laux, C. O., Spence, T. G., Kruger, C. H., & Zare R N 2003 *Plasma Sources Sci. Technol.* **12** 125–38
[36] Paris P, Aints M, Valk F, Plank T, Haljaste A, Kozlov K V and Wagner H E 2005 *J. Phys. D. Appl. Phys.* **38** 3894–9
[37] Griem H R 2005 *Principles of plasma spectroscopy* (Cambridge University Press)
[38] Griem H R 1961 Plasma spectroscopy
[39] Calzada M D, Moisan M, Gamero a. and Sola a. 1996 *J. Appl. Phys.* **80** 46
[40] van der Mullen J A M 1990 *Phys. Rep.* **191** 109–220
[41] Sáinz A, Margot J, García M C and Calzada M D 2005 *J. Appl. Phys.* **97** 113305
[42] Xiong, Q., Nikiforov, A. Y., González, M. A., Leys, C., & Lu X P 2013 *Plasma Sources Sci. Technol.*

Plasma Sources Sci. Technol **22** 15011–3
[43] NIST Atomic Spectra Database
[44] Babaeva N Y and Kushner M J 2014 *Plasma Sources Sci. Technol.* **23** 15007
[45] Laroussi M 2015 *IEEE Trans. Plasma Sci.* **43** 703–12
[46] Park G Y, Park S J, Choi M Y, Koo I G, Byun J H, Hong J W, ... and Lee J K 2012 *Plasma Sources Sci. Technol.* **21** 43001
[47] Laroussi M, Tendero C, Lu X, Alla S and Hynes W L 2006 *Plasma Process. Polym.* **3** 470–3
[48] Herrmann H W, Henins I, Park J and Selwyn G S 1999 *Phys. Plasmas* **6** 2284–9
[49] Weltmann K D, Kindel E, Brandenburg R, Meyer C, Bussiahn R, Wilke C and von Woedtke T 2009 *Contrib. to Plasma Phys.* **49** 631–40
[50] Bussiahn R, Brandenburg R, Gerling T, Kindel E, Lange H, Lembke N, Weltmann K D, Von Woedtke T and Kocher T 2010 *Appl. Phys. Lett.* **96** 143701
[51] Uhm H S, Lim J P and Li S Z 2007 *Appl. Phys. Lett.* **90** 1–4
[52] Deng X, Shi J and Kong M G 2006 *IEEE Trans. Plasma Sci.* **34** 1310–6
[53] Norberg S A, Johnsen E and Kushner M J 2015 *J. Appl. Phys.* **118** 013301
[54] Darny T, Pouvesle J, Puech V, Douat C, Dozias S and Robert E 2017 *Plasma Sources Sci. Technol.* **26** 45008
[55] Yonemori S and Ono R 2014 *J. Phys. D. Appl. Phys.* **47** 125401
[56] Goree J, Liu B, Drake D and Stoffels E *IEEE Trans. Plasma Sci.* **34** 2010–1
[57] Schneider S, Lackmann J W, Ellerweg D, Denis B, Narberhaus F, Bandow J E and Benedikt J 2012 *Plasma Process. Polym.* **9** 561–8
[58] Schneider, S., Lackmann, J. W., Narberhaus, F., Bandow, J. E., Denis, B., & Benedikt J 2011 *J. Phys. D. Appl. Phys.* **44** 379501
[59] Mai-prochnow A, Murphy A B, Mclean K M, Kong M G and Ken K 2014 *Int. J. Antimicrob. Agents* **43** 508–17